On hybrid residual distribution–Galerkin discretizations for steady and time dependent viscous laminar flows

Dobeš, Jiři ; Ricchiuto, Mario ; Abgrall, Rémi ; Deconinck, Herman

Abstract: This paper is concerned with the extension of second order residual distribution (RD) schemes to time dependent viscous flows. We provide a critical analysis of the use of a hybrid RD-Galerkin approach for both steady and time dependent problems. In particular, as in Ricchiuto (2008) and Villedieu etal. (2011), we study the coupling of a Residual Distribution (RD) discretization of the advection operator with a Galerkin approximation for the second order derivatives, with a Peclet dependent modulation of the upwinding introduced by the RD scheme. The final objective is to be able to achieve uniform second order of accuracy with respect to variations of the mesh size or, equivalently, of the local Peclet/Reynolds number. Starting from the scalar formulation given in the second order case in Ricchiuto etal. (2008), we perform an accuracy and stability analysis to extend the approach to time-dependent problems, and provide thorough numerical validation of the theoretical results. The schemes, formally extended to the system of laminar Navier-Stokes equations, are also compared to a finite volume scheme with least-squares linear reconstruction on the solution of standard test problems. While the scalar tests show the potential of this approach in providing uniform accuracy w.r.t. the range of values of the Peclet/Reynolds number, the results for the laminar Navier-Stokes equations show that in practice, the use of Peclet number based corrections does not change dramatically the quality of the solutions obtained. This justifies the quest for new formulations.

DOI: https://doi.org/10.1016/j.cma.2014.09.002

On hybrid residual distribution-Galerkin disretizations for steady and time dependent viscous laminar flows

Jiří Dobeš[a], Mario Ricchiuto[b,*], Rémi Abgrall[c] and Herman Deconinck[d]

[a] Doosan Skoda Power
Tylova 1/57 Plzen, 301 28 Czech Republic

[b] Inria Bordeaux Sud-Ouest
200 avenue de la Vieille tour, 33405 Talence cedex, France

[c] Institute of Mathematics, University of Zurich
Winterthurerstrasse 190 CH8057 Zurich, Switzerland

[d] von Karman Institute for Fluid Dynamics
Chausse de Waterloo, 72, B-1640 Rhode-St-Gense Belgium

[*] Corresponding author :
Email : mario.ricchiuto@inria.fr
Phone : +33 5 24 57 41 17
Fax : +33 5 24 57 40 38

August 23, 2014

Abstract

This paper is concerned with the extension of second order residual distribution (RD) schemes to time dependent viscous flows. We provide a critical analysis of the use of a hybrid RD-Galerkin approach for both steady and time dependent problems. In particular, as in (Ricchiuto et al. J.Comp.Appl.Math. 215, 2008, Villedieu et al. J.Comput.Phys, 230, 2011), we study the coupling of a Residual Distribution (RD) discretization of the advection operator with a Galerkin approximation for the second order derivatives, with a Peclet dependent modulation of the upwinding introduced by the RD scheme. The final objective is to be able to achieve uniform second order of accuracy with respect to variations of the mesh size or, equivalently, of the local Peclet/Reynolds number. Starting from the scalar formulation given in the second order case in (Ricchiuto et al. J.Comp.Appl.Math. 215, 2008), we perform an accuracy and stability analysis to extend the approach to time-dependent problems, and provide thorough numerical validation of the theoretical results. The schemes, formally extended to the system of laminar Navier-Stokes equations, are also compared to a finite volume scheme with least-squares linear reconstruction on the solution of standard test problems. While the scalar tests show the potential of this approach in providing uniform accuracy w.r.t. the range of values of the Peclet/Reynolds number, the results for the laminar Navier-Stokes equations show that in practice, the use of Peclet number based corrections does not change dramatically the quality of the solutions obtained. This justifies the quest for new formulations.

Contents

Introduction and problem setting

This paper studies a class of second order discretizations for the simulation of compressible laminar flows. In absence of physical viscosity, the schemes considered reduce to the Residual Distribution (RD) schemes developed in the last decades by various groups. Reviews of the RD approach can be found in [2, 13]. When diffusion is present, the approach used for several years is to invoke a finite element analogy [12] (see also [26]), and add to the upwind distribution of the advective residual a Galerkin approximation of

the diffusion operator [25, 36, 34, 35]. Several applications of this hybrid discretization are shown in [32].

As remarked in [23, 29], this approach is not satisfactory because its accuracy is not uniform over the whole range of values of the mesh size, viscosity, local speeds. In particular, while on relatively coarse meshes second order is indeed obtained in practice, as one consider finer meshes only first order rates are observed.

To cure this flaw, three possibilities exist in literature. One is to look for a edge-continuous approximation of the solution derivatives, e.g. by means of a gradient reconstruction [11, 23] ; the second consists in rewriting the scalar advection equation as a first-order hyperbolic differential system [22] which is discretized using standard RD schemes. The objective of this paper, is to study a third approach, proposed in [29, 37]. In this method, RD is re-cast as a stabilized Galerkin discretization. By analogy with what is done in the SUPG and GLS case [19, 18], in [29, 37] a dependence of the stabilization term on the cell Peclet/Reynolds number is introduced so that in diffusion dominated regions the full Galerkin scheme is recovered, while the hybrid method is used in high Reynolds regions.

The scope of this paper is to give further insight into this approach, extend it to the time dependent case, and show its applications to the laminar Navier-Stokes calculations. Our results show that, while in the scalar case one can clearly show that this approach allows to recover a uniform second order convergence rate, for moderate/high Reynolds laminar flows its beneficial effects are much less pronounced even when looking at friction coefficients. This justifies the quest for new consistent approaches allowing to further reduce the discretization error in viscous flows [21, 22, 3, 4, 5].

The structure of the paper is the following. In section §1 we review the basics of the methodology proposed in [28, 29] and describe its extension to laminar Navier-Stokes simulations. Some numerical experiments on steady problems are then discussed in section §2. These tests are meant to asses the accuracy obtained with different definitions of the stabilization parameter as a function of the local Peclet/Reynolds number for both scalar advection-diffusion and laminar flows. The extension to time dependent simulations is described in detail in section §3, and tested on various problems in section §4. The paper is ended by a summary of the results and suggestions for future work.

1 Discretization of the flow equations : steady case

1.1 Scalar advection diffusion equation

The starting point for this study is the advection diffusion equation

$$\vec{\lambda} \cdot \nabla u = \nabla \cdot (\nu \nabla u) \quad \text{on} \quad \Omega \subset \mathbb{R}^2 \,. \tag{1}$$

This equation is discretized on an unstructured triangulation of the spatial domain Ω composed by a set non-overlapping triangular elements E, whose area will be denoted by $|E|$. Let h denote the reference size of the mesh (e.g. largest element diameter), and let u_h denote the standard P^1 continuous Lagrange finite element approximation of the nodal values of u on the mesh. In this paper we only consider the two dimensional case, but the extension to three space dimensions is straightforward.

The prototype discrete model studied in this paper is obtained via the following steps :

1. **Discrete advection :** a discrete advection operator is obtained by first computing on each element the residual $\varphi^{\mathrm{a},E}$

$$\varphi^{\mathrm{a},E} = \int_E \vec{\lambda} \cdot \nabla u_h \, dx \,, \tag{2}$$

and then by splitting $\varphi^{\mathrm{a},E}$ to the three forming nodes of element E. When u_h is piecewise linear, denoting the nodal values by $\{u_j\}_{j\in E}$, one easily shows that [25]

$$\varphi^{\mathrm{a},E} = \sum_{j\in E} k_j u_j \,, \tag{3}$$

where the k_js are the *so-called* upwind parameters defined as

$$k_j = \frac{\vec{\lambda}\cdot\vec{n}_j}{2}\,, \tag{4}$$

with $\vec{n}_j$ the inward normal to the face opposite to node j scaled by the length of the face. The splitting of the advective residual is obtained by means of *distribution coefficients* β_i^{a}. Several definitions are possible. A very common choice is the one leading to the *multidimentional upwind* LDA scheme defined by [25, 24]

$$\varphi_i^{\mathrm{a,LDA}} = \beta_i^{\mathrm{LDA}}\varphi^{\mathrm{a},E}, \qquad \beta_i^{\mathrm{LDA}} = \frac{k_i^+}{\sum_{j\in E} k_j^+}\,. \tag{5}$$

The Galerkin scheme can also be recast in this formalism [12, 26]

$$\varphi_i^{\mathrm{a,G}} = \int_E \psi_i \lambda\cdot\nabla u_h \, dx = \beta_i^{\mathrm{G}}\varphi^{\mathrm{a},E}, \qquad \beta_i^{\mathrm{G}} = \frac{1}{3}\,, \tag{6}$$

having denoted by ψ_i the basis function corresponding to node i. Other choices can be made, and will be used later in the results section. Their discussion is not interesting for the scopes of this paper, and we refer the interested reader to [2, 13, 15] for mode details.

2. Diffusion : The diffusion operator is approximated by a standard Galerkin weak formulation which in two dimensions, and in the P^1 case, can be written as

$$\int_\Omega \nu\nabla u_h\cdot\nabla\psi_i \, dx = \sum_{E|i\in E} \varphi_i^{\mathrm{d,G}}\,, \quad \varphi_i^{\mathrm{d,G}} = \nu\sum_{j\in E}\frac{\vec{n}_i\cdot\vec{n}_j}{4|E|}u_j\,. \tag{7}$$

3. Peclet dependence : Following [29, 37], a coupling between the discrete advective and diffusive residuals is introduced by means of a blending function of the local *flow regime*, measured by the cell Peclet/Reynolds number :

$$Pe^E = \frac{\|\lambda\| h_E}{\nu}\,, \tag{8}$$

with h_E a cell mesh size, e.g. its external diameter. This leads to the following local nodal residual

$$\begin{gathered}\varphi_i^E = [1-\xi(Pe)]\varphi_i^{\mathrm{a,G}} + \xi(Pe)\xi(Pe)\varphi_i^{a,\mathrm{RD}} + \varphi_i^{\mathrm{d,G}} = \beta_i^*\varphi^{\mathrm{a},E} + \varphi_i^{\mathrm{d,G}} \\ \beta_i^* = [1-\xi(Pe)]\beta^{\mathrm{G}} + \xi(Pe)\beta_i^{\mathrm{RD}}\end{gathered}\;; \tag{9}$$

Nodal equations : nodal equations are obtained by assembling contributions from all the elements surrounding a node as

$$0 = \sum_{E|\,i\in E}\varphi_i^E = \sum_{E|\,i\in E}\left(\beta_i^*\varphi^{\mathrm{a},E} + \varphi_i^{\mathrm{d,G}}\right) \tag{10}$$

which can be solved by means of some relaxation procedure. Classically, in the RD literature one makes use of the explicit pseudo time stepping iteration [25, 24]

$$u_i^{n+1} = u_i^n - \alpha_i \sum_{E|\, i\in E} \varphi_i^E \,, \tag{11}$$

with α_i a relaxation parameter having dimensions of a time step over the square of the mesh size.

A key element in the above procedure is the definition of the cell Peclet number. In [28, 29] the authors suggest the following definition (in d spatial dimensions) :

$$Pe^E = \frac{\|\lambda\|_{L^2} h^{dD}}{\nu}, \qquad h^{2D} = 2\sqrt{\frac{|E|}{\pi}}, \qquad h^{3D} = \sqrt[3]{3\frac{|E|}{4\pi}}\,, \tag{12}$$

based on the use of the external circle (ball in 3D) diameter for the local mesh size, and of the standard L^2 norm of the local velocity. Another approach is to define a Peclet number based on the ratio of the local advective and diffusive cell residuals as :

$$Pe^E = \frac{\int_E \lambda\cdot\nabla u \,\mathrm{d}x}{\int_E \nu \Delta u_{xx}} \approx \frac{|E|\|\lambda\|\frac{\delta u}{h}}{|E|\nu\frac{\delta u}{h^2}} \approx \frac{\|\lambda\| h}{\nu}, \tag{13}$$

where δu represents a characteristic value of the variation of the solution u over the element. The advantage of this approach is, that it is not necessary to determine velocity and the characteristic size element. The problem is that in the P^1 case it is not clear how to evaluate the diffusive element residual on the denominator of the last expression. Following [33], in [37] the authors suggest to use some norms of the nodal residuals to this effect. The choice of the norm is not unique, but in practice the results are quite independent on this choice. Possible definitions obtained with this approach are

$$Pe_1^E = \frac{\sum_{i\in E}|\varphi_i^{\mathrm{a}}|}{\sum_{i\in E}|\varphi_i^{\mathrm{d,G}}|}, \qquad Pe_2^E = \sqrt{\frac{\sum_{i\in E}(\varphi_i^{\mathrm{a}})^2}{\sum_{i\in E}(\varphi_i^{\mathrm{d,G}})^2}}\,. \tag{14}$$

Numerical tests show that the two definitions give nearly identical results. Here we will make use of the first definition, based on a L^1-like norm.

Once a definition of the local Peclet number has been chosen, one must define the blending functions $\xi(\cdot)$ in (9). The basic idea behind this approach is that the Galerkin scheme should be recovered for small Pe, while the hybrid scheme should be used for large values of this parameter. So the blending function should verify The blending coefficient has to be chosen such that

$$\lim_{Pe\to 0}\xi(Pe) = 0, \qquad \lim_{Pe\to\infty}\xi(Pe) = 1. \tag{15}$$

Actually, in practice the main requirement is that for fine enough meshes one should have $|\xi(Pe^E)| \le C_E h$ for some bounded constant C_E (cf. [17, 33] for more details). Several choices are possible, a very simple one is

$$\xi(Pe) = \max(1, Pe)\,. \tag{16}$$

The problem with this simple definition is that the hybrid scheme is recovered as soon as $Pe \ge 1$, leading to poor accuracy in regions where the advective and diffusive effects are equally important.

To derive a different definition of the blending coefficient, we examine the 1D time dependent version of scheme (11), taking $\alpha_i = \Delta t/\Delta x$, and assuming $\lambda > 0$ for simplicity :

$$\frac{u_i^{n+1}-u_i^n}{\Delta t} = -\xi\lambda\frac{u_i^n - u_{i-1}^n}{\Delta x} - (1-\xi)\lambda\frac{u_{i+1}^n - u_{i-1}^n}{2\Delta x} + \nu\frac{u_{i+1}^n - 2u_i^n + u_{i-1}^n}{\Delta x^2}\,. \tag{17}$$

The idea is now to look at the L^∞ stability of the above iteration. To do this, we recast the last equation as :

$$u_i^{n+1} = c_0 u_i^n + c_{+1} u_{i+1}^n + c_{-1} u_{i-1}^n \,, \tag{18}$$

where

$$c_{+1} = \frac{\lambda \Delta t}{2\Delta x}(\frac{2}{Pe} - 1 + \xi) \qquad c_{-1} = \frac{\lambda \Delta t}{2\Delta x}(\frac{2}{Pe} + 1 + \xi)$$

$$c_0 = 1 - \frac{\lambda \Delta t}{\Delta x}(\xi + \frac{2}{Pe})$$

with $Pe = \lambda \Delta x / \nu$. One easily checks that $c_0 + c_{+1} + c_{-1} = 1$. For the scheme to verify the positive coefficient criterion, and hence a discrete maximum principle, we now require that $c_0 \geq 0$, $c_1 \geq 0$, $c_{-1} \geq 0$. The first condition gives us a time step restriction

$$\Delta t \leq \frac{1}{\xi \dfrac{\lambda}{\Delta x} + 2\dfrac{\nu}{\Delta x^2}} \,, \tag{19}$$

while the last condition is always satisfied. Finally, the second condition can be used to provide a definition of the blending parameter. In particular, $c_{+1} \geq 0$ requires

$$\xi \geq 1 - \frac{2}{Pe} \,, \tag{20}$$

which allows to use the Galerkin scheme in a much larger region than just $Pe < 1$. In practice, we can take

$$\xi(Pe) = \max(0, 1 - \frac{2}{Pe}). \tag{21}$$

Note that a similar analysis can be performed also in two space dimensions, but only provided some particular assumptions are made on the topology of the triangulation (e.g. purely hexagonal meshes, diagonally cut quadrilaterals, etc.), and on the relaxation iterations chosen. The main result of this analysis would be a finer definition of the type

$$\xi(Pe^E) = \max(0, 1 - \frac{\alpha^E}{Pe^E})$$

for some constant α^E depending on the topology of the triangulation. This analysis is omitted here for brevity. In the numerical tests that follows we will simply use the value $\alpha^E = 2$ as suggested by the one dimensional analysis.

1.2 Discretization of the laminar viscous flow equations

We present a short description of the extension of the schemes to the system of the Navier-Stokes equations, which is detailed in [25, 36, 34, 35, 37].

The schemes are formally extended to systems of equations. The advection residual (2) is now replaced by the integral of the divergence of the inviscid fluxes

$$\varphi^{\mathrm{a},E} = \int_E \nabla \cdot \mathrm{F}_h(u_h)\, dx \,, \tag{22}$$

with u_h now the array of conserved quantities (mass, momentum, and energy density), and F_h some edge continuous polynomial approximation of the flux, built upon the values of the linear approximation of u_h. As in the scalar case, several choices exist for the

splitting of $\varphi^{\mathrm{a},E}$. For example, when F_h is linear, the Galerkin scheme reduces again to a centered spliting, giving in two space dimensions :

$$\beta_i^{\mathrm{G}} = \frac{1}{3}\mathbf{I}_4\,, \tag{23}$$

with $\mathbf{I}_4$ the 4×4 identity matrix. A similar matrix extension of mane other schemes exists [34]. The LDA scheme (5) is obtained by replacing the scalar upwind parameters (4) by the projection of the Jacobian matrices of the Euler equations onto the edge normals $\vec{n}_j$. The LDA distribution matrix is then defined by (cf. equation (5))

$$\beta_i^{\mathrm{LDA}} = k_i^+\big(\sum_{j\in E} k_j^+\big)^{-1} \tag{24}$$

where now the positive part of the k_j matrices is computed by standard eigenvalue decomposition. Conditions on the existence of the inverse matrix $\big(\sum_{j\in E} k_j^+\big)^{-1}$, and its meaning in singular points, are given in [1]. Many other possibilities exist. A detailed description is not interesting for our scopes, and we refer to [2, 13, 15] for details. Concerning the discrete viscous operator, still denoted by $\varphi_i^{\mathrm{d,G}}$, a standard evaluation of the Galerkin variational integral is adopted, as explained e.g. in [25, 36, 34, 35].

Viscous and inviscid operators are coupled by means of a scalar blending function ξ depending on the Peclet number now computed generalizing the first expression in (14) as

$$Pe = \frac{\sum_{i\in E}\|\varphi_i^{\mathrm{a}}\|_{L_2}}{\sum_{i\in E}\|\varphi_i^{\mathrm{d,G}}\|_{L_2}}. \tag{25}$$

In the last equation, the operator $\|\varphi\|_{L_2}$ denotes the Euclidean L^2 norm of the residual vectors φ. The final discretization can be written as (cf. equation (9))

$$\sum_{E|i\in E}\varphi_i^* = 0\,, \qquad \varphi_i^* = \xi(Pe)\varphi_i^{\mathrm{RD}} + \big(1-\xi(Pe)\big)\frac{1}{3}\mathbf{I}_4\varphi^{\mathrm{a},E} + \varphi_i^{\mathrm{d,G}}\,, \tag{26}$$

with $\xi(\cdot)$ defined as in (21).

For the laminar Navier-Stokes equations we have compared the results obtained with the hybrid RD-Galerkin schemes with those of a *cell centered* Finite Volume (FV) scheme developed in [14]. The solver is based on a cell centered approximation, with a linear least square reconstruction and the limiter introduced in [8] as a option. All the computations have been performed using Roe's numerical flux solver [30]. The discretization of viscous fluxes is done on dual grid interpolating solution values from element centers to nodes, and approximating the derivatives on auxiliary volumes connecting centroids of the cell with mesh vertices. The interested reader is referred to [14] and references therein for mode details.

2 Numerical experiments for steady problems

2.1 Scalar advection-diffusion

We consider the test proposed in [23]. The steady advection-diffusion equation is solved on the spatial domain $[0,1]^2$, with $\vec{\lambda} = (\lambda_x, \lambda_y) = (0,1)$, and $\nu = 0.01$. The exact solution can be easily computed, and is given by

$$u = -\cos(2\pi\eta)\exp\Big(\frac{\zeta(1-\sqrt{1+16\pi^2\nu^2})}{2\nu}\Big)\,, \tag{27}$$

with $\eta = \lambda_y x - \lambda_x y$, and $\zeta = \lambda_x x + \lambda_y y$. We compute discrete solutions on a sequence of unstructured meshes. The mesh sizes are choses such that the range of the mesh Peclet number $Pe = \|\lambda\| h/\nu$, is $Pe = [0.33, 10]$, containing the most interesting region $Pe \approx 1$.

The results are summarized on figure 1. In the figure, the two pictures on the top and the bottom-left one, represent the error convergence curves relative to three different approaches : hybrid without Peclet dependent blending, on the top-left ; blending based on the approach suggested in [28, 29] (equations (12), and (16)), referred to as older modification, on the top-right ; the modified approach suggested here (equations (13), and (21)), referred to as new modification, on the bottom-left. The last picture on the bottom-right shows a comparison of the convergence of the L^2 norm of the error for the three different approaches.

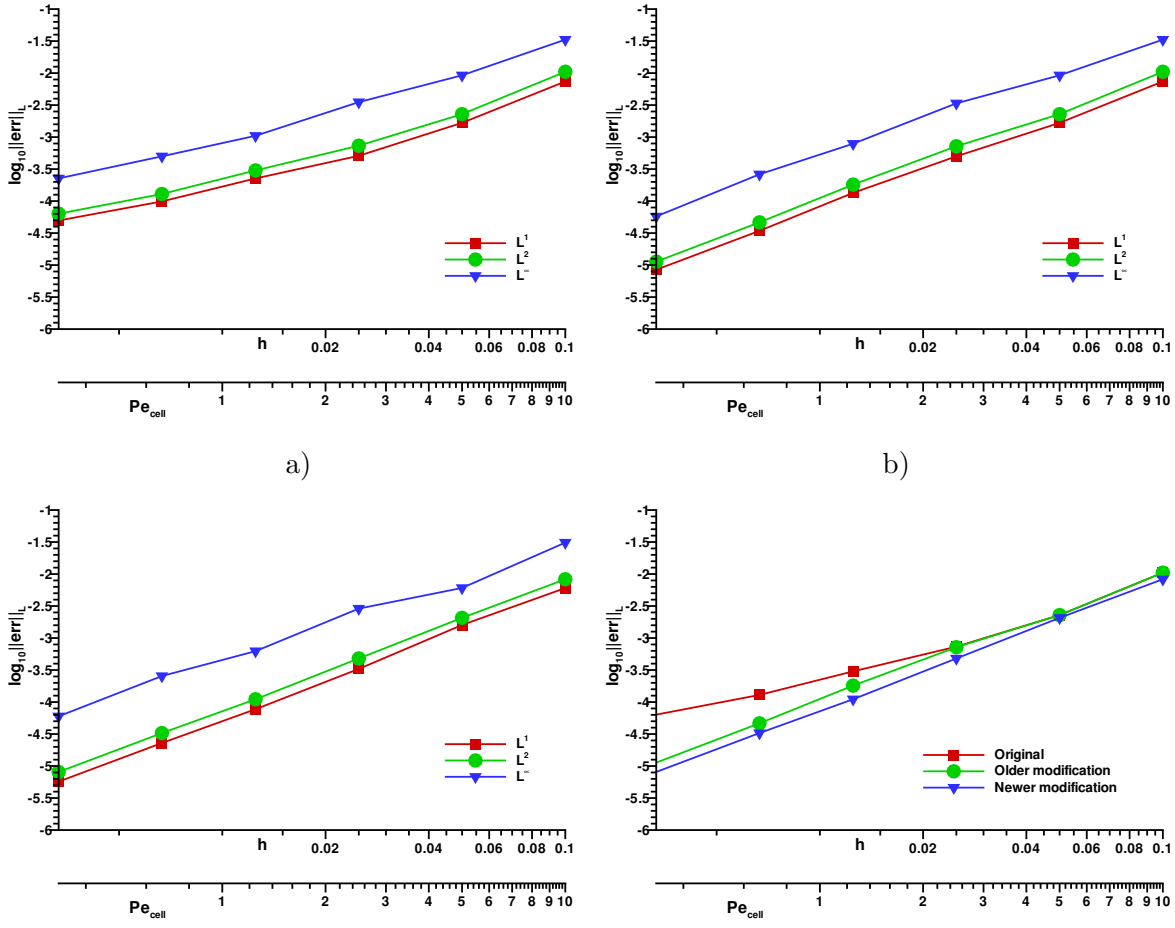

Figure 1: 2D advection-diffusion equation, test eq. (27). a) Hybrid scheme without Pe dependence ($\xi = 1$) ; b) modification of the distribution coefficients given by (12), and (16) (older modification) c) modification of the distribution coefficients given by (13), and (21) (newer modification). d) comparison of different formulations in L^2 norm.

From the first three figures, one can see that different error norms give roughly the same asymptotic behavior, with a slightly more pronounced irregular L^∞ convergence for the new approach, probably due to an increased sensitivity to mesh irregularities

related to the used of local residuals in the definition of he Peclet (13). The L^1 and L^2 norms, however, show a very similar nice monotone convergence of the error also for the new approach. The last picture shows similar trends to those already reported in [23, 28, 29, 37]. The original, Peclet independent, hybrid formulation is flawed by a reduction of the convergence rates, which is cured by the modifications proposed in [28, 29], and here. In particular, the definition of the Peclet and of the blending function (13) and (21) do allow further reduce the error w.r.t. the formulas proposed in [28, 29].

2.2 Laminar flat plate boundary layer

We consider now the classical flat plate boundary layer flow. For the derivation of the semi-analytical solution, due to Blasius, one can refer to the textbooks by White [40] or Schlichting [31]. Besides the velocity profile, for our purposes we will be interested in the behavior of the friction coefficient

$$c_f = \frac{\tau_w}{\frac{1}{2}\rho_e u_e^2}, \qquad \tau_w = \nu \left.\frac{\partial u}{\partial y}\right|_{y=0}, \tag{28}$$

which for Blasius' solution can be shown to be

$$c_f = \frac{\left.\frac{\partial u}{\partial y}\right|_w}{\sqrt{Re_x}}, \qquad Re_x = \frac{u_e x}{\nu}, \qquad \left.\frac{\partial u}{\partial y}\right|_w = 0.664067\,. \tag{29}$$

We consider and incoming flow haracterized by a Mach number $Ma = 0.3$, and by a Reynolds number based on the length of the flat plate $Re \approx 2 \cdot 10^5$. This corresponds to the following free stream conditions: $\rho_\infty = 1.4$, $u_\infty = 0.3$, $p_\infty = 1$, $\nu = 1.5 \cdot 10^{-6}$. In the model we have used classical perfect gas equations of state, and Sutherland's law for the viscosity.

For the set up of the simulations, we have followed the NPARC Alliance Validation Archive `www.grc.nasa.gov/WWW/wind/valid/fplam/fplam.html`. In particular, equally spaced grid points are placed along the plate, while in the vertical direction the points are placed at constant η coordinates, where

$$\eta = \frac{y}{\sqrt{\frac{u_\infty}{2\nu x}}}, \tag{30}$$

with the grid evenly spaced until $\eta = 4$ and then stretched by a factor of 1.1 until the outer boundary at $\eta = 50$ is reached. For $x < 0.3$ the y coordinate is the same as $x = 0.3$. The final grid resolution is 52×35 elements. There are 13 nodes in the x direction prior to leading edge of the flat plate. The thus generated in composed of quadrilaterals which are then diagonally cut (up-runinng diagonals) to obtain a triangulation. A picture of the initial quadrilateral grid is reported on figure 2.

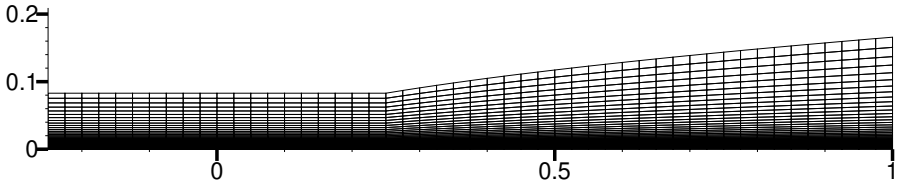

Figure 2: Mesh for laminar incompressible flow over a flat plate

Several simulations have been run with both linear and high (second) order nonlinear RD splittings of the inviscid terms. In particular, we have tested the linear LDA scheme

(cf. sections §1.1 and §1.2), the nonlinear blended Bx scheme of [15], and the nonlinear N-modified scheme of [7] (see also [27]). The interested reader is referred to original publications for details concerning these schemes. For comparison, finite volume computations have been also performed. To be fair to both the RD and FV schemes, these have been run both on the quadrilateral and triangulated meshes, with and without limiter.

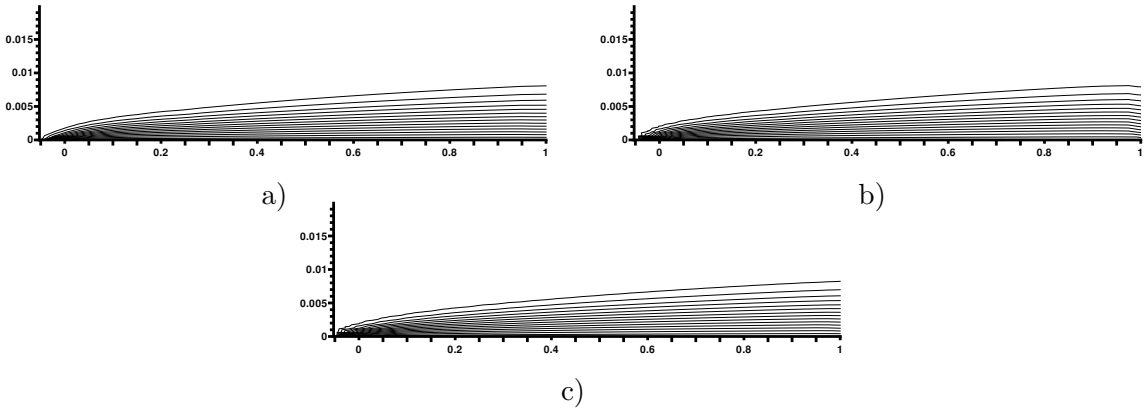

Figure 3: Laminar flat plate boundary layer : isolines of Mach number. Linear second order FV scheme on quads (a), and on triangles (b). Linear RDscheme on triangles (c).

The results are summarized on figures 3, 4, and 5. In particular, in the first we report pictures showing the qualitative capturing of the development of the boundary layer. It is interesting to note that, while the FV scheme on quads (top-left picture) is the one providing the smoothest solution in vicinity of the leading edge of the plate, on triangles, with the same boundary conditions, a perturbation appears in vicinity of the outlet (top-right picture). This shows a grid dependence absent in the RD solution (bottom picture).

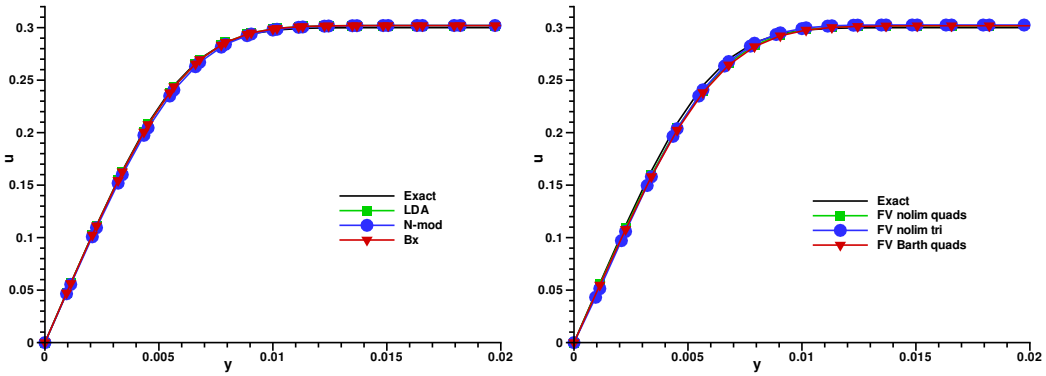

Figure 4: Laminar flat plate boundary layer : velocity profiles at $x = 0.8$. Comparison with semi-analytical solution of Blasius (exact). Left : RD schemes. Right : FV schemes.

The results obtained for different choices of the RD splitting, and with or without the FV limiter, are quite similar. This can be clearly seen in the vertical velocity profiles at $x = 0.8$ compared to the semi-analytical solution in figure 4. The pictures show that, while all RD results give a very close approximation of the theoretical profile at this station, all

FV results give a slight deviation from the theory, with an under-prediction of the slope. The slope error has an effect on the friction coefficient c_f, whose profile along the plate is shown in figure 5. The figure shows a large error in c_f in the FV solutions on triangles (right-picture), certainly related to the outlet perturbation seen in figure 3. The pictures show that the FV solution on triangles has a large deviation from the theoretical solution, with considerable under-prediction of the coefficient. The FV results on quadrilaterals and the RDones are more comparable, with the FV seemingly remaining closer to the theoretical profile even at stations more upstream, and the RDgiving a slightly better result at intermediate stations.

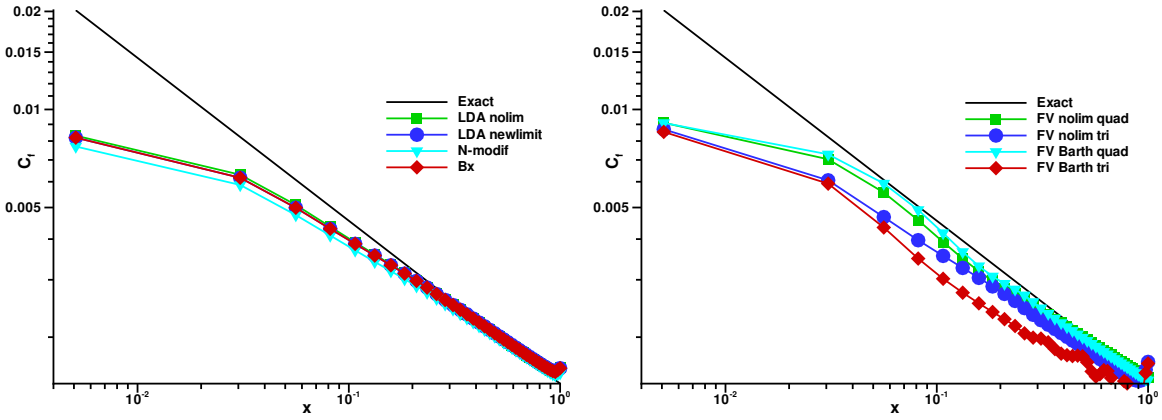

Figure 5: Laminar flat plate boundary layer : distribution of the friction coefficient along the plate. Comparison with semi-analytical solution of Blasius (exact in the figures). Left : RD schemes. Right : FV schemes.

For RD, the results are practically unaffected by the Pe dependent correction. This behavior is understood by looking at the vertical distribution of cell Pe and blending parameter at $x = 0.8$, where both velocity profile and c_f are well resolved. The profile, shown on figure 6, shows that $\xi(Pe)$ is practically always above 0.5, and the blending is active in few cells, so that its overall effect is very mild. While very close to the wall this effect might be reduced by using definitions of the cell Reynolds number similar to (12), but this would still give a negligible difference (e.g. for $y \leq 0.008$ in figure 6) w.r.t. the hybrid formulation obtained for $\xi = 1$.

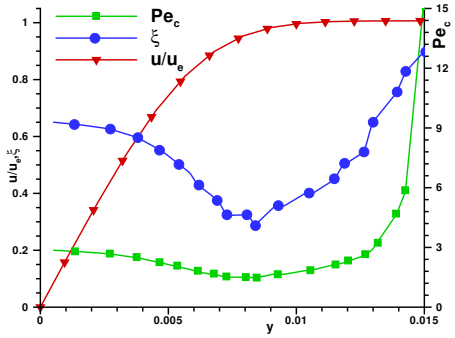

Figure 6: Cell Peclet number and blending coefficient ξ vertical profiles at $x = 0.8$.

2.3 Supersonic flow past a NACA0012 airfoil

Before analyzing the time dependent case, we consider one more steady test involving a shock. The test is taken from [9], and consists of a supersonic flow past a NACA0012 airfoil. The free-stream Mach and Reynolds numbers are $Ma = 2$, and $Re = 106$ respectively. The angle of attack is $\alpha = 10°$. Ww will compare on this test the hybrid discretization obtained splitting the inviscid part of the system with the nonlinear Bx scheme of [15] with and without the Peclet dependent correction.

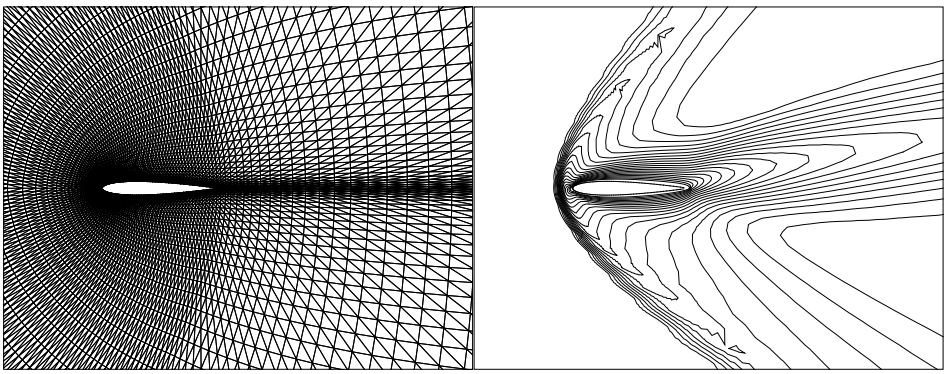

Figure 7: Supersonic flow past a NACA 0012 airfoil. Left : mesh. Right : Mach isolines.

The computational mesh is shown on the left on figure 7. On the right in the same figure we report the isolines of the Mach number, showing the qualitative behavior of the numerical solution. The contour plots of the two formulations (with and without Pe correction) are nearly undistinguishable, and only one (with the correction) is reported. To try to visualize the differences between the two solutions we report on figure 8 the friction coefficient, and the distribution of the Mach number and of the density along the stagnation line. The Peclet correction leads to a slightly sharper shock, and to a small increase in the deceleration at the stagnation point, as well as of the acceleration acceleration on the suction side, The differences, however, are really minor.

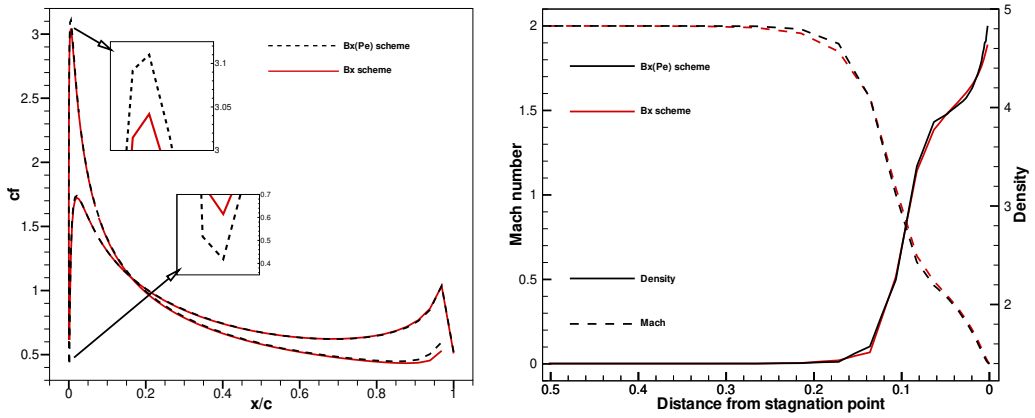

Figure 8: Supersonic flow past a NACA 0012 airfoil. Left : friction coefficient. Right : Mach and density distribution along the stagnation line.

3 Time dependent problems

3.1 Unsteady scalar advection-diffusion : discrete prototype

We now study the time-dependent problem

$$u_t + \vec{\lambda} \cdot \nabla u = \nu \Delta u. \tag{31}$$

The prototype scheme considered can still be written as in (10), except that now the time derivative is included in the elemental integrals, as in classical stabilized finite elements methods. As before, the local nodal contribution is will be defined as

$$\varphi_i = \varphi_i^{\mathrm{a,G}} + \varphi_i^{\mathrm{d,G}} + \xi(\varphi_i^{\mathrm{a,RD}} - \varphi_i^{\mathrm{a,G}}), \tag{32}$$

where all the φ_i^{a} now include both the advection terms and the time derivative. For example, in two space dimensions and for pure advection, one easily finds that the local nodal contribution of the Galerkin is

$$\varphi_i^{\mathrm{a,G}} = \frac{|E|}{3} \sum_{j \in E} \left(\frac{1 + \delta_{ij}}{4} \frac{\partial u_j}{\partial t} \right) + \frac{1}{3} \varphi^{\mathrm{a},E}\,, \tag{33}$$

with $\varphi^{\mathrm{a},E}$ still defined as in (2). The full contribution for advection diffusion is obtained by adding the term $\varphi_i^{\mathrm{d,G}}$, still defined as in (7).

The time dependent extensions upwind discretizations, such as the LDA scheme introduced in section §1.1, can be obtained by means of a Petrov-Galerkin analogy introduced in [12, 20, 16], and widely used afterwards (see e.g. [6, 26]). The simplest description of this analogy is that RD schemes are recast from the Galerkin scheme obtained by means of a cell-wise constant perturbation of the test functions. These perturbations turn out to have a simple dependence on the distribution coefficients, and the resulting test functions read locally

$$\tilde{\psi}_i \Big|_E = \psi_i \Big|_E + \beta_i^{\mathrm{a}} - \frac{1}{3}$$

Application of a Petrov-Galerkin variational statement leads to the local nodal contributions :

$$\varphi_i^{\mathrm{a,E}} = \frac{|E|}{3} \left(\beta_i^{\mathrm{a}} + \frac{1}{6} \right) \frac{\partial u_i}{\partial t} + \frac{|E|}{3} \sum_{\substack{j \in E \\ j \neq i}} \left[\left(\beta_j^{\mathrm{a}} - \frac{1}{12} \right) \frac{\partial u_j}{\partial t} \right] + \beta_i^{\mathrm{a}} \varphi^{\mathrm{a},E}. \tag{34}$$

Fully discrete equations are then obtained by choosing a time integration scheme, and monotone discretizations can be designed e.g. by locally blending with appropriate mass lumped schemes. The interested reader ca refer for details to [6, 15, 26] and references therein. For advection-diffusion, we once more want to study the hybrid scheme

$$\sum_{E | i \in E} \varphi_i^* = 0\,, \qquad \varphi_i^* = \xi(Pe)\varphi_i^{\mathrm{a,E}} + (1 - \xi(Pe))\varphi_i^{\mathrm{a,G}} + \varphi_i^{\mathrm{d,G}}\,. \tag{35}$$

The objective of the rest of the paper is to verify that this prototype has potential to provide second order accurate schemes for time dependent problems, and to verify this potential numerically, both for the advection-diffusion equation, and for the laminar Navier-Stokes equations. Note, in particular, that the extension to systems is obtained introducing a matrix formalism, as already illustrated for the steady case. One can refer to the description and to the references given in section §1.2 for more details.

In the next section we will analyze the one dimensional case. The study allows to justify the use of this hybrid formulation in the time dependent case, and to justify the choice of parameters used later in the computations.

3.2 Hybrid upwind-central scheme in one space dimension

We consider the analysis of the one dimensional case, for which scheme (35) reduces to a hybrid upwind-central discretization. We will focus on the discrete equations obtained when integrating in time with the second order Crank-Nicholson scheme, but a similar analysis can be performed for different choices. Also, we will assume, without loss of generality, that the advection speed verifies the hypotheses :

$$\lambda > 0\,, \quad \lambda = \mathcal{O}(1)\,.$$

We start from the Galerkin scheme which can been written as

$$\frac{1}{6}\Delta^n u_{i-1} + \frac{2}{3}\Delta^n u_i + \frac{1}{6}\Delta^n u_{i+1} + \frac{\lambda\Delta t}{\Delta x}\left[\frac{u_{i+1}-u_{i-1}}{2} - \frac{1}{Pe}(u_{i+1}-2u_i+u_{i-1})\right]^{n+1/2} = 0\,, \quad (36)$$

having set $\Delta^n u = u^{n+1} - u^n$, and $u^{n+1/2} = (u^{n+1}+u^n)/2$. With a similar notation, in one dimension the hybrid upwind-central diffusion scheme reads :

$$\frac{5}{12}\Delta^n u_{i-1} + \frac{2}{3}\Delta^n u_i - \frac{1}{12}\Delta^n u_{i+1} + \frac{\lambda\Delta t}{\Delta x}\left[u_i - u_{i-1} - \frac{1}{Pe}(u_{i+1}-2u_i+u_{i-1})\right]^{n+1/2} = 0\,. \quad (37)$$

As done in the steady case, we consider a blending of the two, by means of the parameter ξ function of the Peclet number $Pe = \lambda\Delta x/\nu$:

$$\frac{2+3\xi(Pe)}{12}\Delta^n u_{i-1} + \frac{2}{3}\Delta^n u_i \frac{2-3\xi(Pe)}{12}\Delta^n u_{i+1} + \frac{\lambda\Delta t}{\Delta x}\xi(Pe)(u_i-u_{i-1})^{n+1/2} + \frac{\lambda\Delta t}{\Delta x}\frac{1-\xi(Pe)}{2}(u_{i+1}-u_{i-1})^{n+1/2} - \frac{\lambda\Delta t}{\Delta x}\frac{1}{Pe}(u_{i+1}-2u_i+u_{i-1})^{n+1/2} = 0\,. \quad (38)$$

For $\xi = 0$ we recover the Galerkin scheme, while for $\xi = 1$ we recover the hybrid upwind-central discretization. The first question we need to answer is whether this hybrid scheme can reach second order of accuracy, and under which hypotheses. To answer this question, we use the modified equation method. After performing all the Taylor series developments in space and time, and following the procedure in [39], we end up with the modified following equation

$$u_t + \lambda u_x = \nu u_{xx} + \left(\frac{1}{2}\xi\nu\Delta x - \frac{1}{12}\lambda^3\Delta t^2\right)u_{xxx} + \left(-\xi\frac{1}{24}\lambda\Delta x^3 + \frac{1}{4}\lambda^2\nu\Delta t^2 - \frac{1}{12}\nu\Delta x^2 + \xi^2\frac{1}{4}\nu\Delta x^2\right)u_{xxxx}. \quad (39)$$

Since the dominating orders in the coefficient in front of the u_{xxxx} term are Δx^2 and Δt^2, the scheme will be second order accurate provided that the coefficient in front of the first term is also less than an order $\mathcal{O}(\Delta x^2 + \Delta t^2)$. To analyze this term, and without loss of generality, we assume that the time step verifies

$$\Delta t = \frac{\sigma}{\dfrac{\lambda}{\Delta x} + \dfrac{\nu}{\Delta x^2}}, \qquad 0 < \sigma \leq 1, \quad \sigma \approx 1\,. \quad (40)$$

Substituting in the first coefficient, we obtain

$$\frac{1}{2}\xi\nu\Delta x - \frac{1}{12}\lambda^3\Delta t^2 = \frac{1}{2}\lambda\Delta x^2\left(\frac{\xi}{Pe} - \underbrace{\frac{1}{6}\frac{\sigma^2 Pe^2}{1+Pe^2}}_{\alpha(Pe)}\right) = \frac{1}{2}\lambda\Delta x^2\left(\frac{\xi(Pe)}{Pe} - \alpha(Pe)\right). \quad (41)$$

We can make the following remarks :

- in the last expression $\alpha(Pe) \leq 1/6$. This means that, given a bounded constant C, for $\xi(Pe) \leq \mathrm{C}Pe$ or equivalently $\xi(Pe) \leq \mathrm{C}\Delta x$, and in particular for the centered scheme obtained for $\xi(Pe) = 0$, we have indeed a second order scheme ;
- if $\xi(Pe) = 1$, the scheme is of order $\Delta x^2/Pe$, which is order one as $Pe = \mathcal{O}(\Delta x)$;
- for $Pe \ll 1$, provided that $\xi(Pe) \leq \mathrm{C}Pe$, with C a bounded constant, the scheme is also second order accurate as $\alpha \to 1/6$ for Pe large enough ;
- if $Pe \ll 1$ then $\alpha(Pe)$ will certainly be negligible, and second order of accuracy is retained, once more provided that $\xi \leq \mathrm{C}Pe$, for a bounded constant C ;
- if $Pe \approx 1$ one sees immediately that if $\xi \leq \mathrm{C}Pe$ for some bounded constant, then $\xi/Pe - \alpha \leq \mathrm{C}$, and once more we find that the scheme is second order accurate.

From the previous observations we gather that a crucial condition is $\xi \leq \mathrm{C}Pe$, which is in practice easy to verify. In particular, for both definitions (16), and (21) we have $\xi \leq Pe$.

To verify if these definitions could somehow be improved or modified in the time dependent case, we again look at the monotonicity of the scheme. As anticipated, this constraint is enforced in RD computations by resorting to properly defined mass lumped formulations in correspondence of discontinuities (see e.g. [15, 26, 6]). So, we consider the mass-lumped version of (38) which reads :

$$\begin{aligned}&\Delta^n u_i + \frac{\lambda\Delta t}{\Delta x}\xi(Pe)(u_i - u_{i-1})^{n+1/2} \\ &\quad + \frac{\lambda\Delta t}{\Delta x}\frac{1-\xi(Pe)}{2}(u_{i+1} - u_{i-1})^{n+1/2} - \frac{\lambda\Delta t}{\Delta x}\frac{1}{Pe}(u_{i+1} - 2u_i + u_{i-1})^{n+1/2} = 0\,. \quad (42)\end{aligned}$$

Last equation is the i-th line of a linear tridiagonal system for the values of the solution at the new time step, which we can compactly write as

$$AU^{n+1} = BU^n$$

For such a system, the conditions for the preservation of extrema in the solution are quite classical, and boil down to requiring that [10]

1. A should be an irreducibly diagonally dominant inverse M-matrix : $a_{ii} \geq 0$, $a_{ij} \leq 0$, and $a_{ii} + \sum_{j\neq i} a_{ij} \geq 0$ with a strict equality at least for one i ;
2. B should be a positive matrix : $b_{ij} \geq 0\ \forall\, i,\, j$.

For (42) we can easily check that

$$A_{i\,i-1} = -\frac{\lambda\Delta t}{4\Delta x}\big(1+\xi+\frac{2}{Pe}\big)\,,\ \ A_{i\,i} = 1+\frac{\lambda\Delta t}{2\Delta x}\big(\xi+\frac{2}{Pe}\big)\,,\ \ A_{i\,i+1} = -\frac{\lambda\Delta t}{4\Delta x}\big(-1+\xi+\frac{2}{Pe}\big)\,,$$

and that

$$B_{i\,i-1} = \frac{\lambda\Delta t}{4\Delta x}\big(1+\xi+\frac{2}{Pe}\big)\,,\ \ B_{i\,i} = 1-\frac{\lambda\Delta t}{2\Delta x}\big(\xi+\frac{2}{Pe}\big)\,,\ \ B_{i\,i+1} = -\frac{\lambda\Delta t}{4\Delta x}\big(-1+\xi+\frac{2}{Pe}\big)\,.$$

One easily checks that $A_{i\,i-1} + A_{i\,i} + A_{i\,i+1} = 1$, and that the conditions we need to satisfy for the preservation of monotonicity are (20), and

$$\Delta t \leq \frac{2}{\xi \dfrac{\lambda}{\Delta x} + 2\dfrac{\nu}{\Delta x^2}}\,. \tag{43}$$

Compared to (19), we have recovered the classical "CFL=2" positivity preservation constraint of the Crank-Nicholson scheme. Note also that (43) is compatible the hypothesis (40) made at the beginning of the analysis.

In conclusion we have shown that, provided that $\xi(Pe)$ is bounded by its argument, and that we satisfy both (20), and a time step constraint, depending on the choice of the time integration scheme, we are able to recover a hybrid discretization which is potentially second order over all the range of values of Pe, and preserves monotonicity under mass lumping.

4 Numerical experiments time dependent problems

In this section we verify numerically the properties of scheme (35). In particular, as done in the steady case, we will first verify its accuracy for a scalar problem. Then, we will test the scheme on laminar flow computations to verify to which extent the introduction of a Peclet dependent hybridization brings an improvement over the simpler, nominally first order, Peclet independent, hybrid scheme. As in the steady case, we will consider three tests : a scalar benchmark with an exact solution, a laminar flow involving the development of a boundary layer, and a laminar flow involving the formation of shocks.

4.1 Unsteady rotational advection-diffusion

In order to be able to perform a grid convergence study, we propose a test for which we are able to derive an analytical solution.

We consider an advection-diffusion equation with $\vec{\lambda} = (\lambda_x, \lambda_y) = (-y, x)$, i.e. a rigid body rotation around the origin with angular velocity $\omega = 1$. We start by looking at the pure diffusion problem in cylindrical coordinates :

$$u_t = \nu \left(u_{rr} + \frac{1}{r} u_r + \frac{1}{r^2} u_{\theta\theta} \right). \tag{44}$$

We now look for a "cylindrical" solution using classical separation of variables. So we take

$$u(t, r) = T(t)\, R(r). \tag{45}$$

The diffusion equation reduces thus to

$$\frac{T'}{T} = \nu \left(\frac{R''}{R} + \frac{1}{r}\frac{R'}{R} \right) = c_1 \tag{46}$$

The solution of $T'/T = c_1$ is simply $T(t) = c_2 \exp(c_1 t)$. The second equation can be recast as a modified Bessel equation

$$r^2 R'' + r R' - r^2 R \frac{c_1}{\nu} = 0\,, \tag{47}$$

which has of the form

$$R(r) = c_3 \mathrm{J}_0(\sqrt{-\frac{c_1}{\nu}}\, r) + c_4 \mathrm{Y}_0(\sqrt{-\frac{c_1}{\nu}}\, r), \tag{48}$$

with J_0 and Y_0 the Bessel functions of the first and second kind. Since Y_0 is singular at the origin, for compatibility with a bounded initial condition we will set $c_4 = 0$. The final solution of the time dependent diffusion problem is thus

$$u(r,t) = c_0 \exp(c_1 t)\, J_0(\sqrt{-\frac{c_1}{\nu}}\, r). \tag{49}$$

We consider now the solution of the advection diffusion equation, which we will simply obtain as the solution of the diffusion equation in the frame of reference rotated with speed $\omega = 1$. To set the integration constants, we choose to impose the maximum value of the solution at the time $t = 2\pi$ (after one revolution) to $u^{2\pi}_{\max} = 0.2$, and the initial maximum to $u^{0}_{\max} = 1$. This leads to the final solution

$$u = \exp(c_1 t)\, J_0(r\sqrt{-\frac{c_1}{\nu}})\,, \qquad \begin{cases} c_1 &= \dfrac{\ln 0.2}{2\pi} \\ r &= \sqrt{\tilde{x}^2 + \tilde{y}^2} \\ \tilde{x} &= x\cos t\alpha + y \sin t\alpha + 0.5 \\ \tilde{y} &= -x \sin t + y \cos t \end{cases} \tag{50}$$

A visualization of the initial solution is reported for completeness on figure 9.

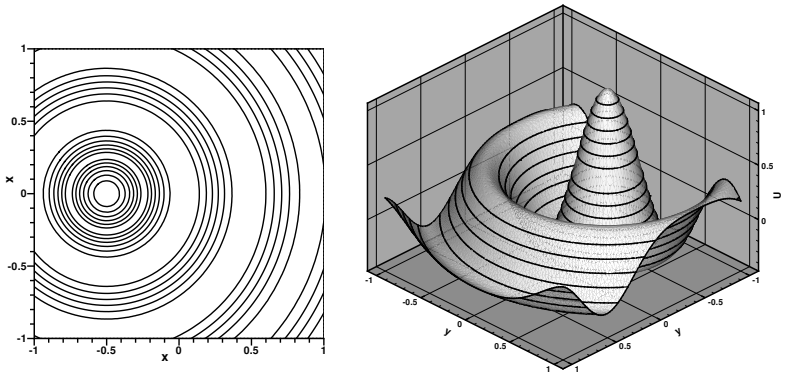

Figure 9: Unsteady rotation-diffusion problem – initial conditions.

We now solve the problem numerically with the hybrid LDA+Galerkin scheme (cf. section §1.1) with and without the Pe dependent correction based on (21), and with the pure Galerkin discretization. Time integration has been performed with the Cranck-Nicholson scheme, guaranteeing the neutral stability of the Galerkin scheme, and the diffusion coefficient has been set to $\nu = 0.005$. Note that the implementation of the initial condition corresponding to (50) quite easy, since the Bessel function is part of the standard C library and can be simply called as `double j0(double x)`.

The results are summarized in figure 10, where we report on the left the plot of the error convergence w.r.t. the mesh size, and the average least-squares convergence rates on the right. The plot confirms that the hybrid scheme is only first order accurate, while the inclusion of the Peclet dependent modification clearly allows to reduce the error, and to increase the convergence rates. Compared to the steady case, the slopes obtained vary between 1.5 and 2.5. While this might be a consequence of the fact that the meshes used in the grid convergence study are not nested but generated independently, it also shows that perhaps better definitions of $\xi(Pe)$ could be used. In particular, the error levels obtained with definitions (14) and (21) are comparable to those of the Galerkin scheme only on the last grids.

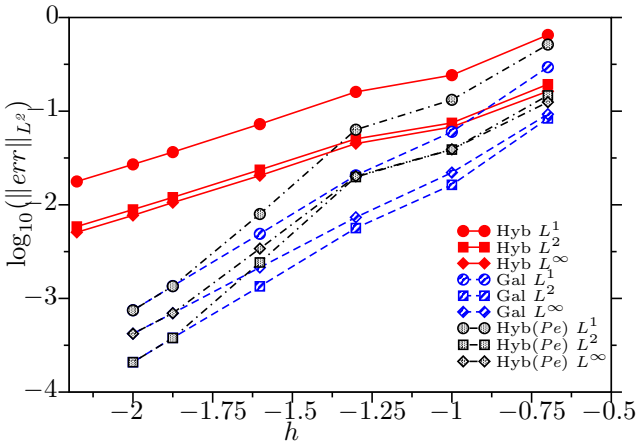

Scheme	L^1	L^2	L^∞
Hybrid	1.03	1.00	1.00
Galerkin	1.96	1.96	1.77
Hybrid + $\xi(Pe)$	2.21	2.23	1.93

Figure 10: Unsteady rotation-diffusion. Error convergence for the hybrid LDA-Galerkin scheme (Hyb), hybrid LDA-Galerkin scheme with Pe dependent blending (Hyb(Pe)), and Galerkin scheme. Left : error plot in log-log scale. Right : Least-squares convergence slopes.

4.2 Laminar flow past a suddenly accelerated wall

We consider the so-called Rayleigh or Rayleigh-Stokes problem, consisting of a suddenly accelerated semi-infinite flat plate [31], with exact solution

$$u = u_\infty \mathrm{erf}(\frac{y}{2\sqrt{\nu t}}). \tag{51}$$

We solve the problem in the time interval $t \in [0, 0.1]$, on domain $\Omega = [0, 1] \times [0, 1]$ with free stream conditions on the top boundary, periodic conditions on the sides, and no-slip wall conditions on the bottom. The free stream condition is given by density, velocity, and pressure equal to $(\rho, u, v, p)_\infty = (1.4, 1, 0, 100)$, with kinematic viscosity set to $\nu = 0.1$.

We use a very coarse triangular mesh with spacing $h = 1/10$ (217 nodes and 392 elements only) on which we compare the schemes obtained with all the RD splittings already tested in section §2.2, and the finite volume scheme. In particular, to be fair to the latter, we have also run FV simulations on a structured Cartesian mesh with the same size. For the RD the influence of the Pe blending (25), (21), and (35) is also studied. A qualitative view of the mesh and of the solution obtained (horizontal velocity isolines) is given on figure 11. Note that in the isoline plots, the same domain is plotted twice to show the periodicity of the solution obtained.

We compare on figure 12 the vertical profiles of the horizontal velocity obtained with the different schemes. The same remarks made in section §2.2 apply here : for the RD results there is practically no influence neither of the choice of the splitting of the inviscid part of the system, nor of the use of the Pe dependent modification. All the results match the analytical solution very well. As for the steady tests, this can be interpreted as a sign that for laminar flows the mesh sizes required to have substantial effects of the Pe dependent hybridization are below those necessary to the RD-Galerkin scheme to resolve correctly the viscous layers. The figure also shows again the poor performance of the FV scheme on triangles compared to both the FV results on quadrilaterals and to the hybrid RD-Galerkin schemes.

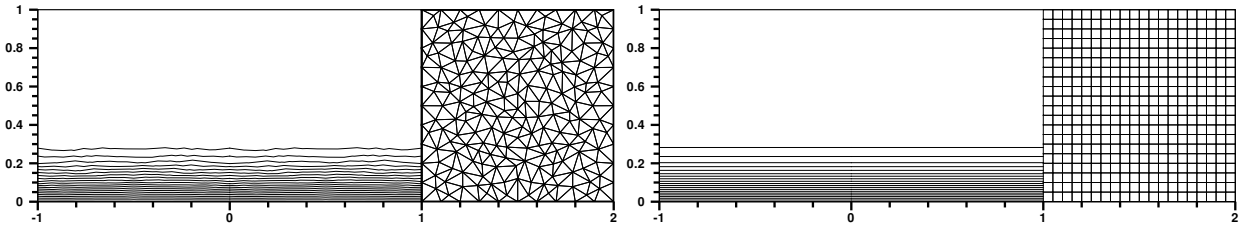

Figure 11: Rayleigh problem. Horizontal velocity isolines at time $t = 0.1$ and mesh. Left pictures : hybrid LDA-Galerkin scheme with Pe dependent modification, unstructured triangles. Right pirctures : second order finite volume without limiter, quadrilateral cells.

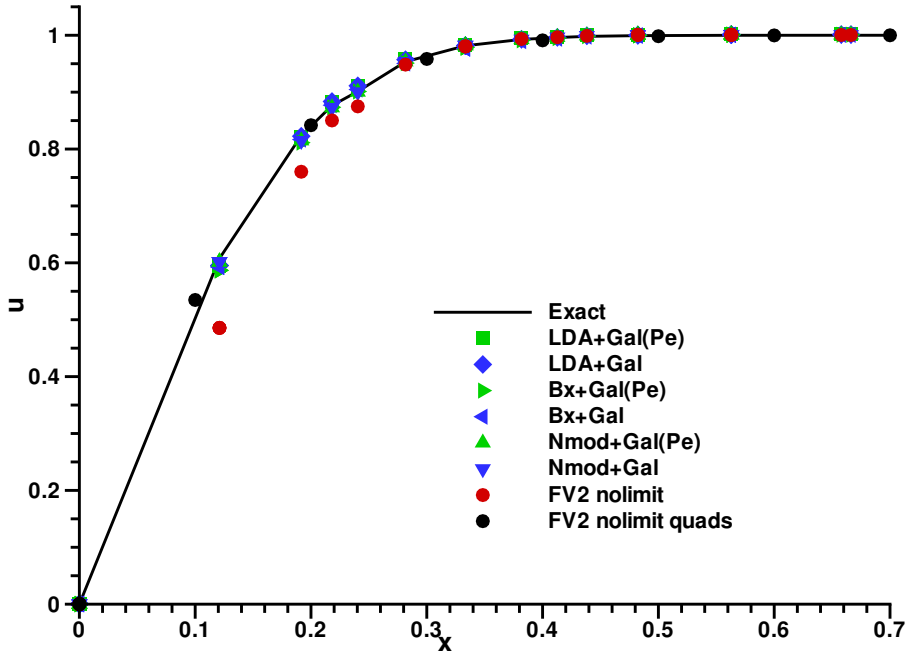

Figure 12: Rayleigh problem. Comparison of computed velocity profiles with the exact solution. Data extracted at $x = 0.5$.

4.3 Vortex shedding past a circular cylinder

To verify the influence of the Pe correction on a more complex case involving the interaction of viscous layers with the external flow, we consider the development of a time dependent von Karman alley behind a circular cylinder, The free stream is characterized by a Mach number of $Ma = 0.1$, and by a Reynolds number of $Re = 100$. Note that laminar vortex shedding starts from $Re \approx 70$, while for $Re \leq 70$ the solution is steady [31]. The mesh used is an unstructured triangulation containing 14,372 elements, with 48 elements placed along the cylinder. The spatial domain extends 8 dimeters away from the cylinder both upstream and sidewise, while it extends 58 diameters downstream.

We discuss the results obtained with the LDA scheme with and without the inclusion

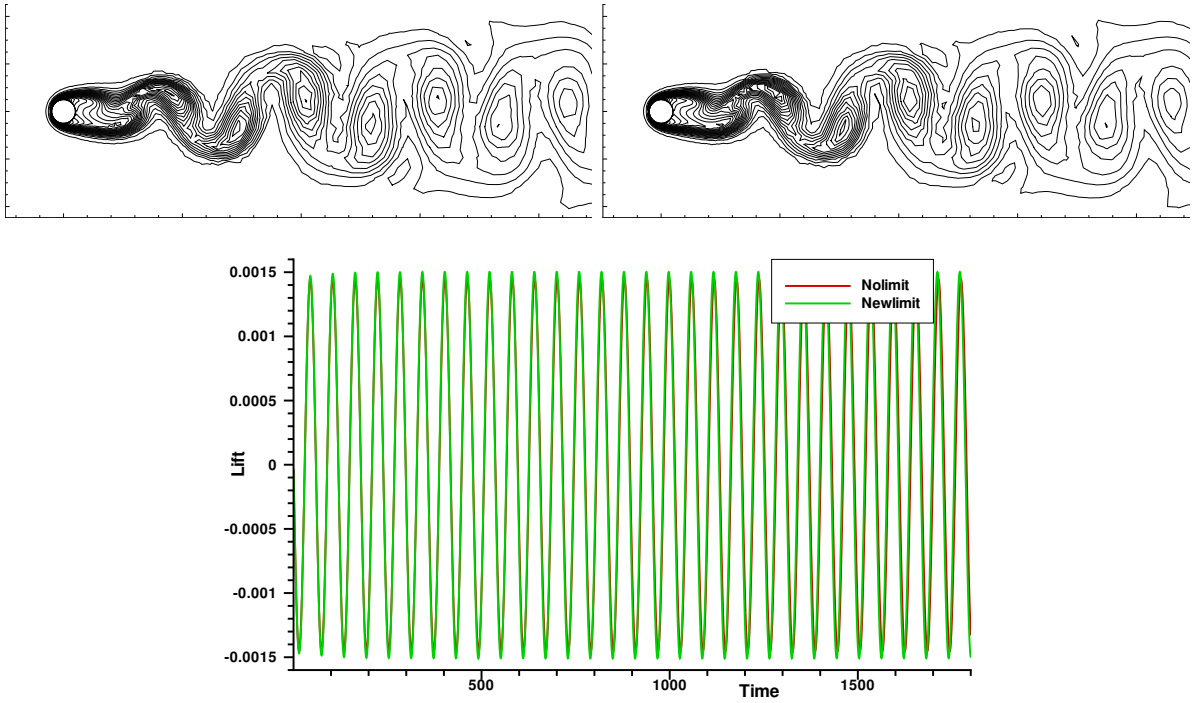

Figure 13: Laminar vortex shedding behind a circular cylinder. Top : isolines of the entropy computed without (left), and with (right) the Pe dependent blending. Bottom : lift force variation in time after periodicity has been achieved

of the Pe dependent blending (25), (21), and (35). We visualize the solutions on figure 13 where we report on top the contour plot of the entropy computed without (left), and with (right) the Pe dependent blending, and on the bottom the variation in time of lift coefficient after periodicity has been attained. Both approaches manage to capture the time dependent shedding of the vortices. A close look at the friction coefficient will reveal a difference in the maximum friction coefficient of the order of 2%, and a slightly more pronounced phase shift in the results without Pe dependent blending, after 25 of the periods visualized. The differences are once again extremely small. We can check again the distribution of the values of the discrete Pe number, shown on figure 14. The map shows that even close to the wall, the smallest value of Pe is higher than 2.

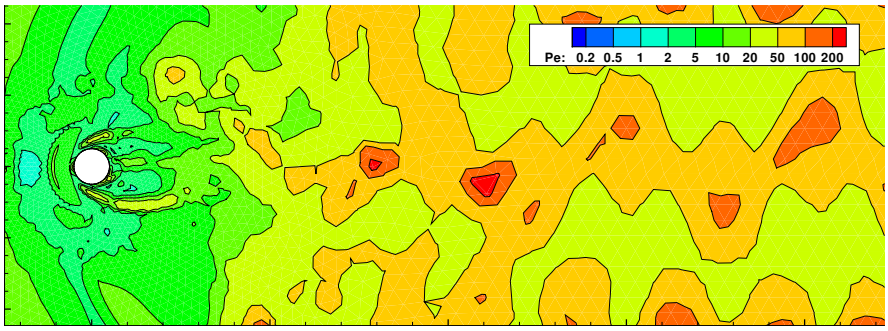

Figure 14: Laminar vortex shedding behind a circular cylinder. Map of the Peclet (25)

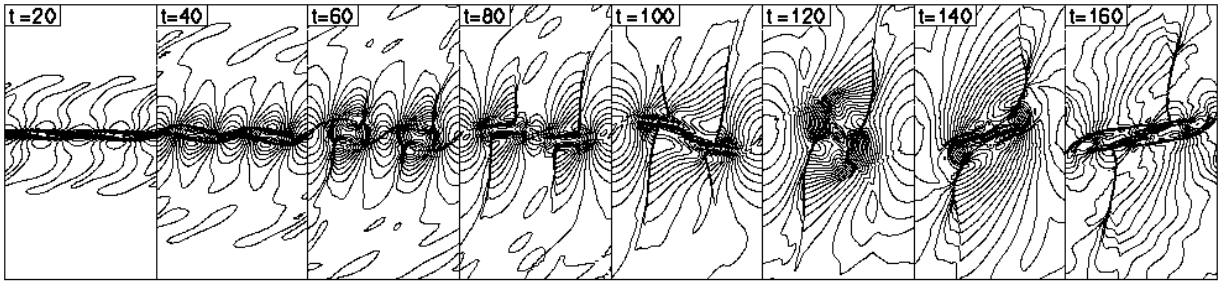

Figure 15: Transonic vortex pairing. Snapshots of the temperature isolines at different times.

4.4 Transonic vortex pairing

As last test, we consider the transonic vortex pairing in a mixing layer [41]. The problem consists of a shear layer defined by two free streams with velocity profiles $u = \tanh(2y)/2$, $v = 0$. To these velocity profiles we superimpose the vertical perturbations

$$v' = \sum_{k=1}^{2} a_k \cos(2\pi k x/L_x + \phi_k) \exp(-y^2/b) \tag{52}$$

with $a_1 = 0.01$, $a_2 = 0.05$, $\phi_1 = \phi_2 = \pi/2$, $b = 10$. A horizontal perturbation u' is computed from condition $\nabla \cdot (u', v') = 0$. The problem has been solved in the domain $[-15, 15] \times [-50, 50]$. The top and bottom boundaries are treated as inviscid walls, and periodic boundary conditions are set on the left and right boundaries. The kinematic viscosity in the free streams is set to $\nu_\infty = 10^{-3}$, corresponding to a Reynolds number $Re = 1000$. The speed of sound (and hence the density) in the initial solution is determined from the assumption of constant stagnation enthalpy

$$a^2 = a_1^2 + \frac{\gamma - 1}{2}(u_1^2 - u) \tag{53}$$

and $Ma_\infty = 0.8$. Constant initial static pressure $p = 1$ is assumed across the whole flow-field. The grid used consists of an isotropic triangulation stretched in the y-direction using the mapping

$$y = \frac{L_y}{2} \frac{\sinh(b_y \eta)}{\sinh(b_y)}, \tag{54}$$

where $\eta \in (-1, 1)$ and $b_y = 3.4$. Two meshes have been used, a 101×101 one containing 10201 nodes and 20000 triangles, and a finer 201×201 triangulation containing 40401 nodes and 80000 triangles A panel showing the development of the vortex pairing over time is reported on figure 15. The pictures show the evolution of the isolines of the temperature computed on the finer grid with the hybrid scheme using the non-oscillatory Bx RD splitting of [15] for the inviscid terms. One can clearly see the formation of two initial vortices pairing up into a larger vortical structure, as well as the appearance of shoclets above each vortex, interacting and deforming the vortical structures, and finally merging into stronger discontinuities.

In figure 16 we report instead the comparison of the temperature field at $t = 160$ obtained on the 101×101 grid with the hybrid Bx-Galerkin scheme (left picture), and with the finite volume scheme (middle picture). The picture shows that both schemes give a nice capturing of the larger vortical structure obtained from the pairing of the two

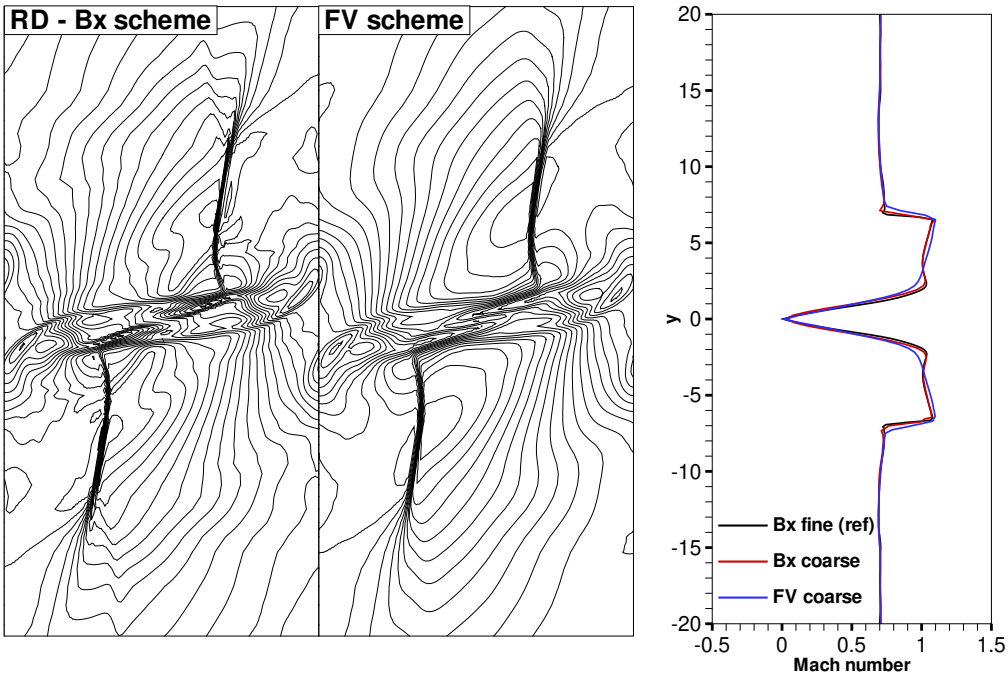

Figure 16: Transonic vortex pairing. Results at $t = 160$. Isolines of temperature obtained with the Bx scheme (left) and with the FV scheme (middle). Right picture : Mach number distribution alon a line cutting through the vertex core and crossing the shocks.

initial vortices. The RD results, however, shows crisper shocks and a richer structure close to the core. To confirm this observation we also report on the right picture in the same figure the distribution of the Mach number along a line with slope 20/30, going through the core, and cutting through the shocks. In the picture we also report, for comparison, the data extracted on the fine mesh computation performed with the Bx scheme. The one dimensional plot shows that already on the coarse mesh the Bx-Galerkin scheme gives a crisper description of the deceleration at the center of the vortical structure.

As for the other cases, we try to visualize the impact of including the Pe blending (25), (21), and (35). This is done on figure 17 where we report the temperature isolines for the hybrid Bx-Galerkin scheme with (left) and without (middle) the Pe correction. The two contour plots can hardly be distinguished, the differences being extremely small. On the rightmost picture, we report the map of the Pe number distribution in the area visualized in the other two images. The picture shows that the region with values of Pe smaller than 2 is very small, thus explaining the negligible impact of the correction.

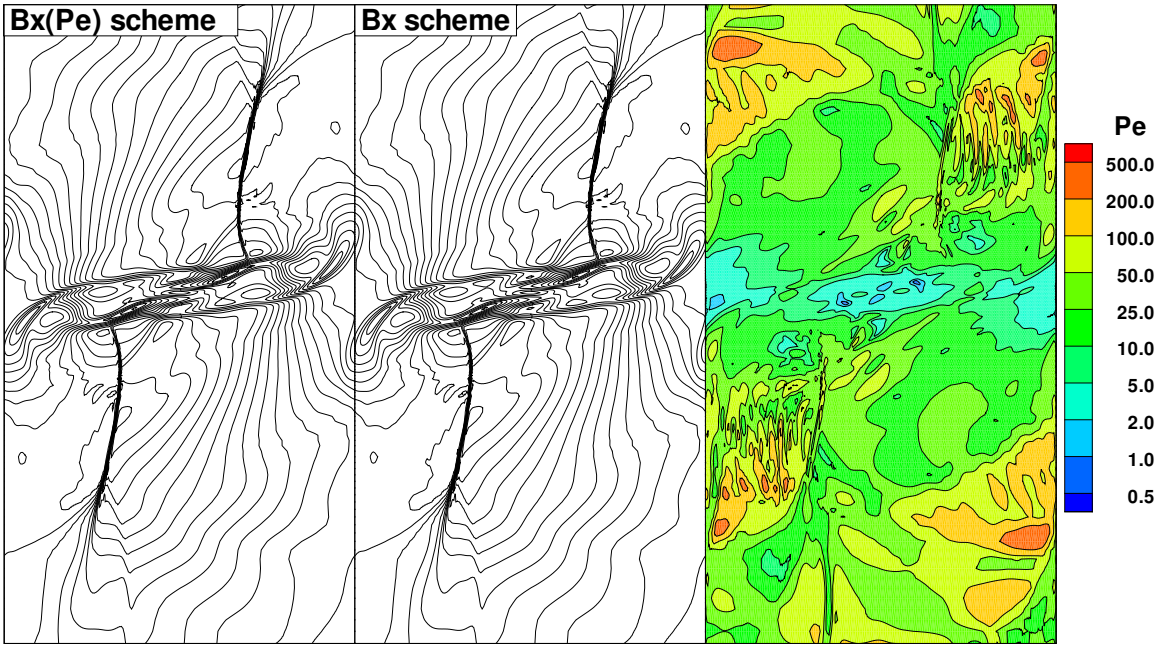

Figure 17: Transonic vortex pairing. Fine mesh results at $t = 160$. Isolines of temperature obtained with the Bx scheme with (left) and without (middle) Pe dependent modification. Right picture : map of local values of Pe.

5 Conclusions

In this paper we have presented a critical review of the approach proposed in the past in [29, 38] to improve the accuracy of hybrid Residual Distribution-Galerkin discretizations of the advection diffusion equation, and of the laminar Navier-Stokes equations. Inspired by what is done in stabilized finite elements, This approach is based on a modulation of the upwinding used in the advective term by a parameter dependent on a local Peclet number. This allows to recover the Galerkin scheme in diffusion dominated (small Peclet) regions. For steady problems, clear improvements in the convergence rates for scalar advection diffusion had been shown in [29], motivating the use of this approach for Navier-Stokes simulations.

In this paper we have reviewed the basics of this approach, and, by means of simple analyses, proposed simple modifications to improve it for steady state computations, and to extend it to unsteady problems. For both the steady and time dependent case, we have performed extensive numerical studies to understand the potential advantages, and the drawbacks of this method. Our study has shown that, while for scalar problems one can easily show a recovery of uniform high order of accuracy over the whole range of values of the local Peclet number, for the laminar Navier-Stokes equations things are quite different. Indeed, we have clearly shown that for these flows the mesh sizes allowing to resolve the viscous layers lead to values of the local Peclet number too high for this approach to make any difference.

On one hand, this is good news for those who have developed in the past hybrid RD-Galerkin codes for laminar flows, as our results show that this hybrid methods performs quite well, providing results as good, and often better, as those of second order finite volume schemes with least squares reconstruction. On the other hand, this means that better solutions to extend RD to viscous flows have to be sought. This justifies the recent investment in genuinely residual based approximations of the viscous terms by H. Nishikawa [21, 22], as well as by some of the authors of the present work [3, 4, 5]. While this new approach might allow a genuine improvement over the hybrid RD-Galerkin formulation. However, the local Pe modulation of the upwind terms might still have some potential in turbulent computations. These topics make the subject of ongoing and foreseen investigations.

References

[1] R. Abgrall. Toward the ultimate conservative scheme: Following the quest. *J.Comput.Phys.*, 167(2):277–315, 2001.

[2] R. Abgrall. A review of residual distribution schemes for hyperbolic and parabolic problems : the july 2010 state of the art. *Comm.Comput.Phys.*, 11:1043–1080, 2012.

[3] R. Abgrall, G. Baurin, D. DeSantis, A. Krutz, and M. Ricchiuto. Numerical approximation of parabolic problems by residual distribution schemes. *Int.J.Num.Meth.Fluids*, 71(9), 2013.

[4] R. Abgrall, D. DeSantis, and M. Ricchiuto. Construction of a high order residual distribution scheme for complex viscous flow. In *Computational Fluid Dynamics 2012, 7th Int. Conf. on Computational Fluid Dynamics, ICCFD7*, 2012. online proceedings: http://www.iccfd.org/iccfd7/proceedings.html.

[5] R. Abgrall, D. DeSantis, and M. Ricchiuto. High-order preserving residual distribution schemes for advection-diffusion scalar problems on arbitrari grids. *SIAM J.Sci.Comp.*, 36:A955–A983, 2014.

[6] R. Abgrall and M. Mezine. Construction of second order accurate monotone and stable residual distribution schemes for unsteady flow problems. *Journal of Computational Physics*, 188:16–55, 2003.

[7] R. Abgrall and M. Mezine. Construction of second-order accurate monotone and stable residual distribution schemes for steady flow problems. *J. Comput. Phys.*, 195:474–507, 2004.

[8] T. J. Barth and D. C. Jesperson. The design and application of upwind schemes on unstructured meshes. AIAA Paper 89–0366, AIAA, Jan 1989.

[9] F. Bassi and S. Rebay. A high-order accurate discontinous finite element method for the numerical solution of the compressible Navier-Stokes equations. *Journal of Computational Phydics*, 131:267–279, 1997.

[10] A. Berman and R. J. Plemmons. *Nonnegative Matrices in the Mathematical Sciences*. Academic Press, 1979.

[11] D. Caraeni and L. Fuchs. Compact third-order multidimensional upwind discretization for steady and unsteady flow simulations. *Computers & Fluids*, 34(4–5):419–441, 2005.

[12] J.-C. Carette, H. Deconinck, H. Paillère, and P.L. Roe. Multidimensional upwinding: its relation to finite elements. *International Journal for Numerical Methods in Fluids*, 20:935–955, 1995.

[13] H. Deconinck and M. Ricchiuto. Residual distribution schemes: foundation and analysis. In E. Stein, R. de Borst, and T.J.R. Hughes, editors, *Encyclopedia of Computational Mechanics*. John Wiley & Sons, Ltd., 2007. DOI: 10.1002/0470091355.ecm054.

[14] J. Dobes. *Numerical Algorithms for the Computation of Unsteady Compressible Flow over Moving Geometries - Application to Fluid-Structure Interaction*. PhD thesis, Université Libre de Bruxelles, 2007.

[15] J. Dobeš and H. Deconinck. Second order blended multidimensional upwind residual distribution scheme for steady and unsteady computations. *Journal of Computational and Applied Mathematics*, 215(2):378 – 389, 2008.

[16] A. Ferrante and H. Deconinck. Solution of the unsteady Euler equations using residual distribution and flux corrected transport. Project Report VKI PR 1997-08, Von Karman Institute for Fluid Dynamics, Belgium, June 1997.

[17] L.P. Franca, S.L. Frey, and T.J.R. Hughes. Stabilized finite element methods: I. application to the advective-diffusive model. *Computer Methods in Applied Mechanics and Engineering*, 95(2):253–276, 1992.

[18] P.L. Franca, S.L. Frey, and T.J.R Hughes. Stabilized finite element methods. i: Application to the advective-diffusive model. *Comp. Meth. Appl. Mech. Engrg.*, 95:253–276, 1992.

[19] T.J.R. Hughes and A. Brook. Streamline upwind Petrov-Galervon karman institute for fluid dynamicsn formulations for convection dominated flows with particular emphasis on the incompressible Navier-Stokes equations. *Comp. Meth. Appl. Mech. Engrg.*, 32:199–259, 1982.

[20] J. Maerz and G. Degrez. Improving time accuracy for residual distribution schemes. Project Report 1996-17, Von Karman Institute for Fluid Dynamics, Belgium, Chausée do Waterloo 72, B-1640 Rhode Saint Genèse, Belgium, June 1996.

[21] H. Nishikawa. A first-order system approach for diffusion equation I: Second-order residual-distribution schemes. *Journal of Computational Physics*, 227(1):315 – 352, 2007.

[22] H. Nishikawa. A first-order system approach for diffusion equation II: Unification of advection and diffusion. *Journal of Computational Physics*, 229(11):3989 – 4016, 2010.

[23] H. Nishikawa and P. Roe. On high-order fluctuation splitting schemes for Navier-Stokes equations. In *ICCFD 3. 3rd Interational Conference on Computational Fluid Dynamics*. Springer-Verlag, 2004.

[24] H. Paillere and H. Deconinck. Compact cell vertex convection schemes on unstructured meshes. In H Deconinck and B Koren, editors, *Notes on Numerical Fluid Mechanics*, pages 1–50. Vieweg-Verlag, Braunschweig, Germany, 1997.

[25] Henri Paillère. *Multidimensional Upwind Residual Distribution Schemes for the Euler and Navier-Stokes Equations on Unstructured Grids*. PhD thesis, Université Libre de Bruxelles, Von Karman Institute for Fluid Dynamics, June 1995.

[26] M. Ricchiuto and R. Abgrall. Explicit runge-kutta residual distribution schemes for time dependent problems: Second order case. *Journal of Computational Physics*, 229(16):5653 – 5691, 2010.

[27] M. Ricchiuto, Á. Csík, and H. Deconinck. Residual distribution for general time dependent conservation laws. *J. Comput. Phys*, 209(1):249–289, 2005.

[28] M. Ricchiuto, N. Villedieu, R. Abgrall, and H. Deconinck. High order residual distribution schemes: Discontinuity capturing crosswind dissipation and extension to advection–diffusion. CFD – High Discretization Methods. VKI Lecture Series 2006–01, Von Karman Institute for Fluid Dynamics, Chausée do Waterloo 72, B-1640 Rhode Saint Genèse, Belgium, 2005.

[29] M. Ricchiuto, N. Villedieu, R. Abgrall, and H. Deconinck. On uniformly high-order accurate residual distribution schemes for advectiondiffusion. *Journal of Computational and Applied Mathematics*, 215(2):287–331, 2008.

[30] P. L. Roe. Approximate Riemann solvers, parameter vectors, and difference schemes. *J. Comput. Phys.*, 43:357–372, 1981.

[31] H. Schlichting. *Boundary-Layer Theory*. Mc-Graw-Hill, seventh edition edition, 1979.

[32] K. Sermeus and H. Deconinck. Drag prediction validation of a multi-dimensional upwind solver. CFD-based aircraft drag prediction and reduction, VKI Lecture Series 2003–02, Von Karman Institute for Fluid Dynamics, Chausée do Waterloo 72, B-1640 Rhode Saint Genèse, Belgium, 2003.

[33] T.E. Tezduyar and Y. Osawa. Finite element stabilization parameters computed from element matrices and vectors. *Computer Methods in Applied Mechanics and Engineering*, 190(3-4):411 – 430, 2000.

[34] E. van der Weide and H. Deconinck. Positive matrix distribution schemes for hyperbolic systems. In *Computational Fluid Dynamics*, pages 747–753, New York, 1996. Wiley.

[35] E. van der Weide and H. Deconinck. Matrix distribution schemes for the system of euler equations. In H. Deconinck and B. Koren, editors, *Euler and Navier-Stokes solvers using multidimensional upwind schemes and multigrid acceleration*, volume 57 of *Notes on Numerical Fluid Dynamics*, pages 113–135. Vieweg, 1997.

[36] E. van der Weide, H. Deconinck, E. Issmann, and G. Degrez. A parallel implicit multidimensional upwind residual distribution method for the Navier-Stokes equations on unstructured grids. *Comp. Mech.*, 23(2):199–208, 1999.

[37] N. Villedieu, T. Quintino, M. Ricchiuto, and H. Deconinck. Third order residual distribution schemes for the Navier-Stokes equations. *Journal of Computational Physics*, 230(11):4301 – 4315, 2011.

[38] N. Villedieu, T. Quintino, M. Ricchiuto, and H. Deconinck. Third order residual distribution schemes for the Navier-Stokes equations. *Journal of Computational Physics*, 230(11):4301 – 4315, 2011. *work performed at the von Karnam Institute.*

[39] R. Warming and Hyett. The modified equation approach to the stability and accuracy analysis of finite-difference methods. *Journal of Copmutational Physics*, (14):159–179, 1974.

[40] F.M. White. *Viscous Fluid Flow.* McGraw-Hill Science/Engineering/Math, 1991.

[41] H. C. Yee, N. D. Sandham, and M. J. Djomehri. Low-dissipative high-order shock-capturing methods using characteriscic-based filters. *Journal of Computational Physics*, 150:199–238, 1999.